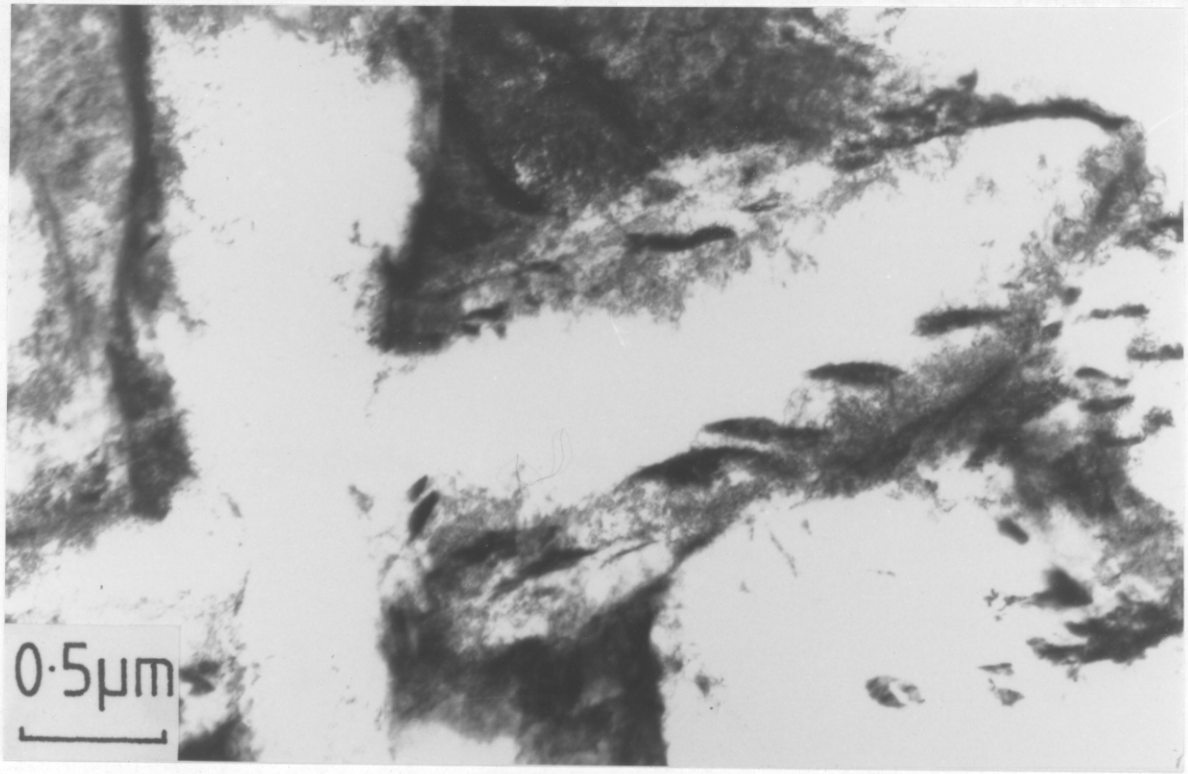

Figure 4.4 (continued).

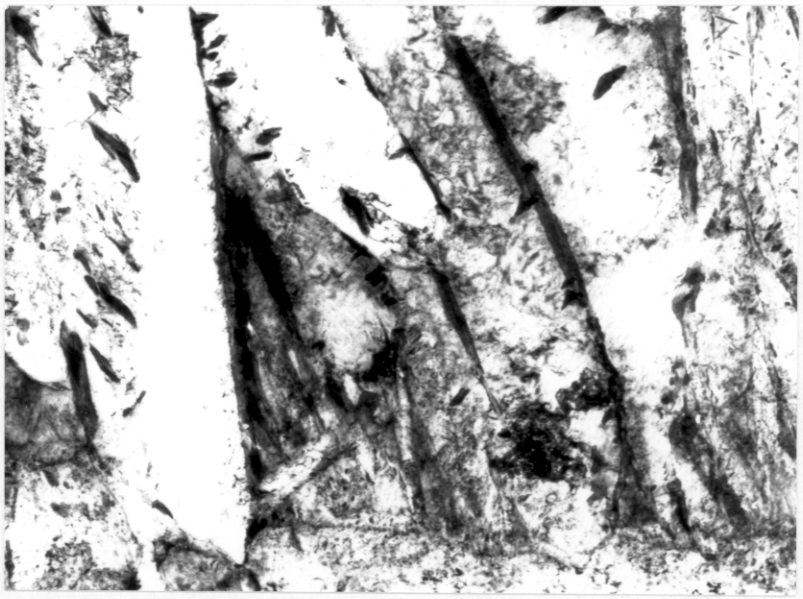

0.5μm

Figure 4.5. Carbides towards the periphery of an acicular ferrite plate.

Figure 4.6. 1.0μm Possible interfacial ledges (arrowed).

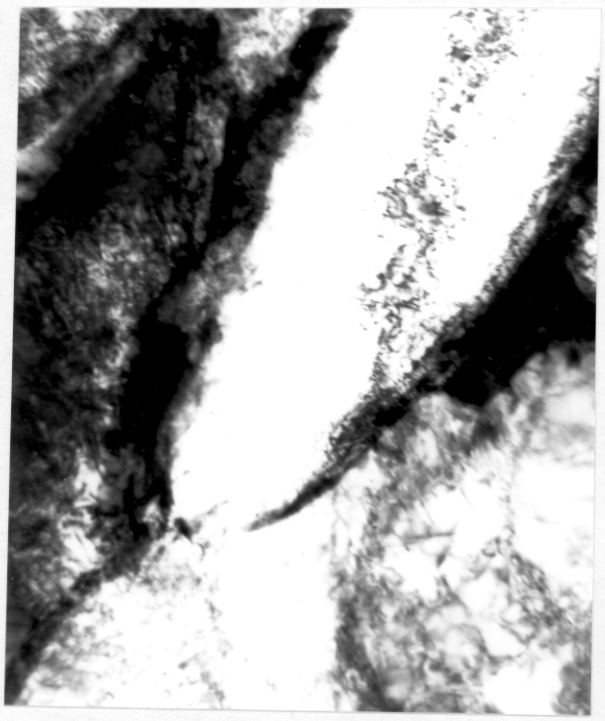

0.25μm

0.15μm

Figure 4.7. Smoothly curved plate tips.

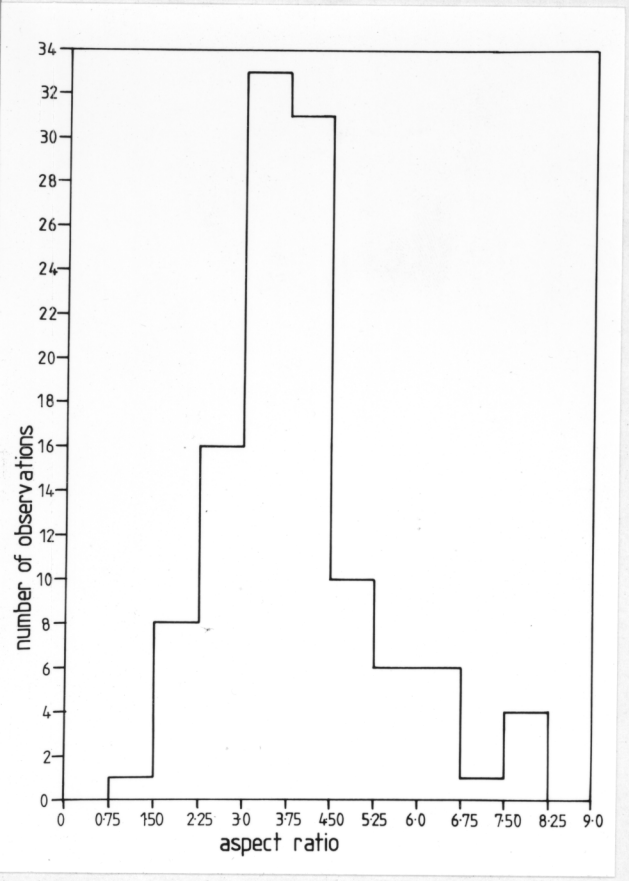

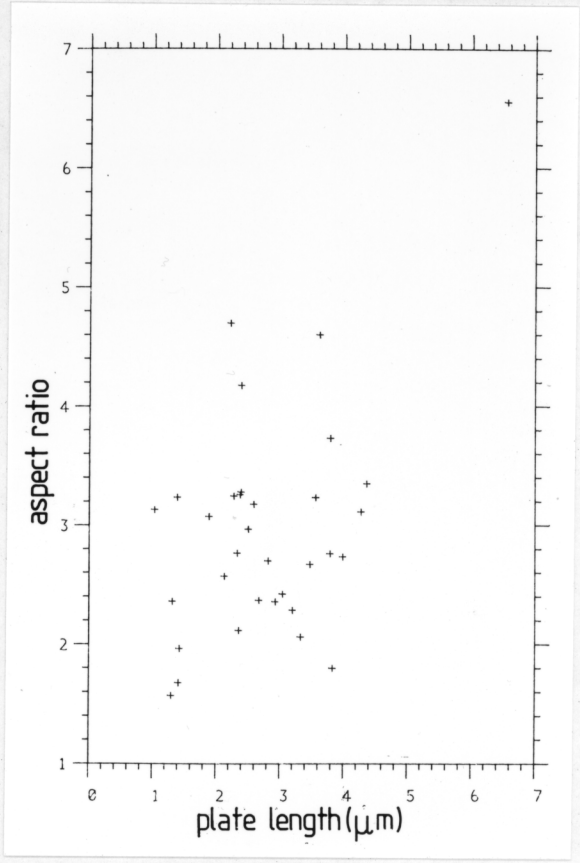

Figure 4.8. Aspect ratios recorded for acicular ferrite plates.

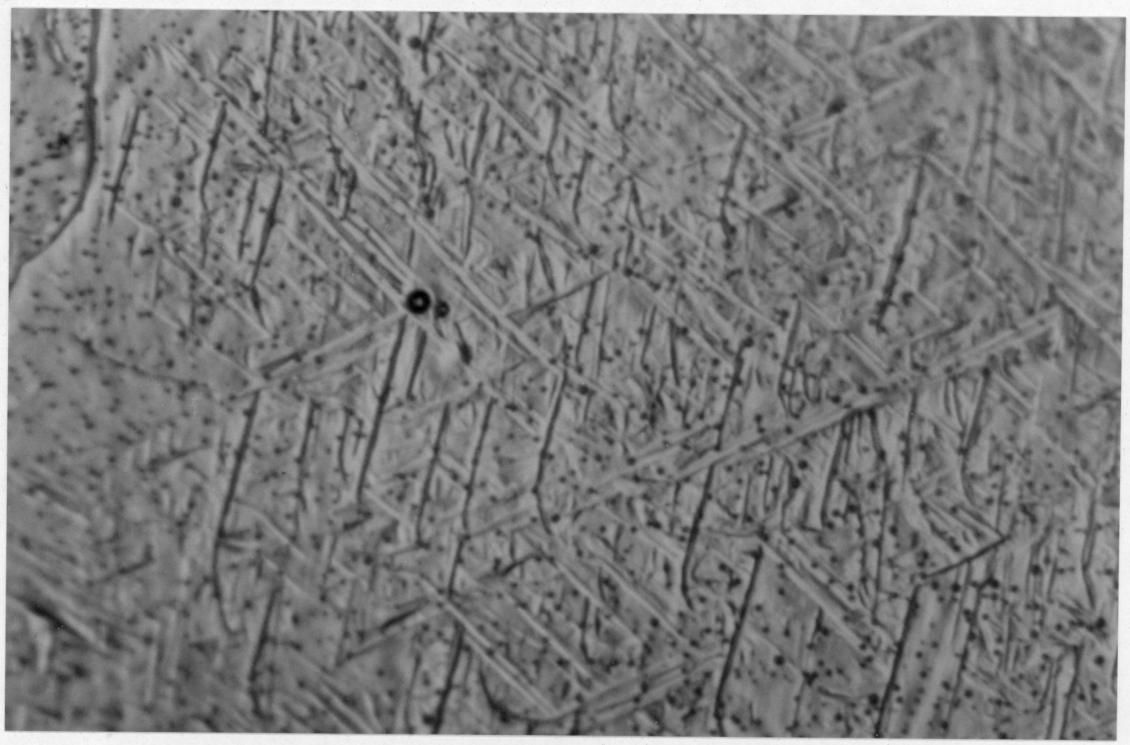

(a) 5.0μm

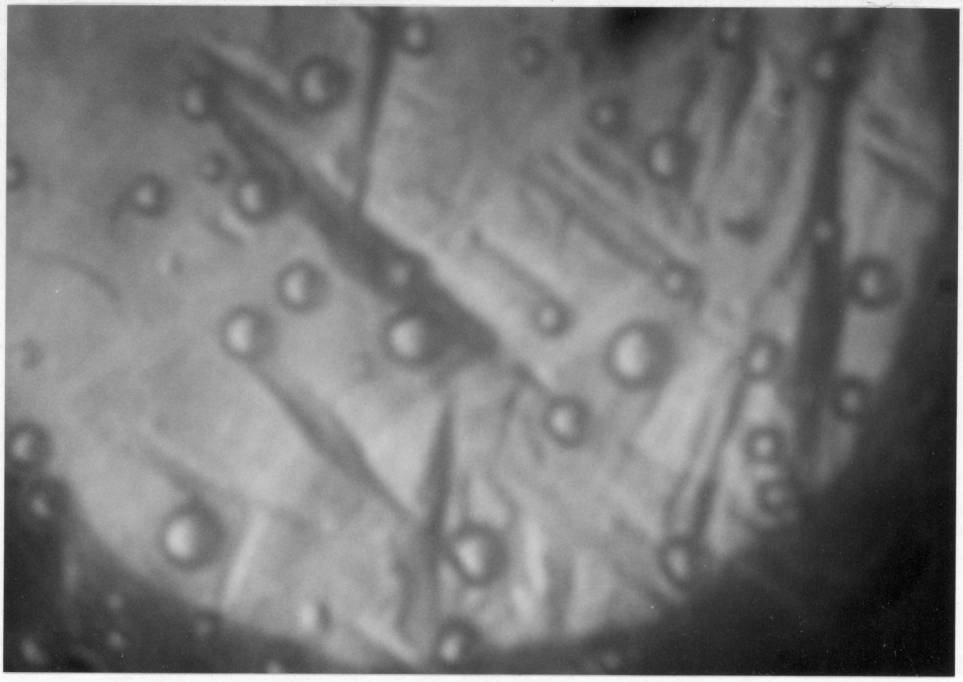

(b) 2.0μm

Figure 4.9. Nomarski interference images of surface relief introduced by acicular ferrite formation, illustrating uniform nature of contrast across a single plate.

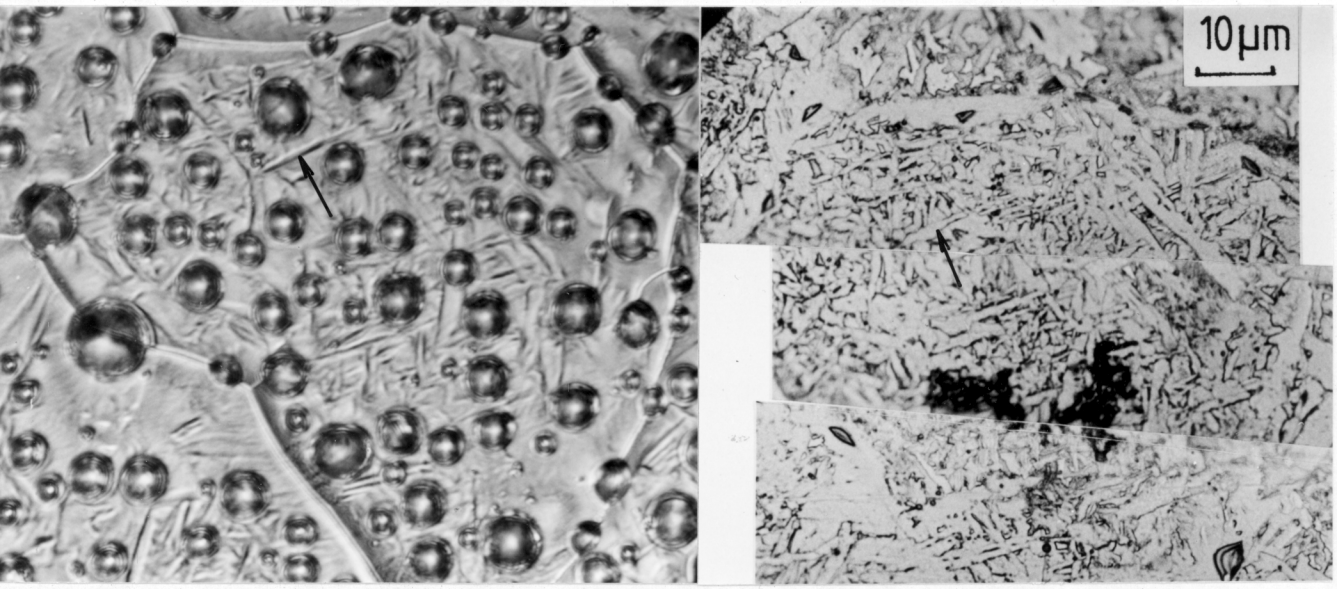

Figure 4.10. Surface relief and underlying microstructure.

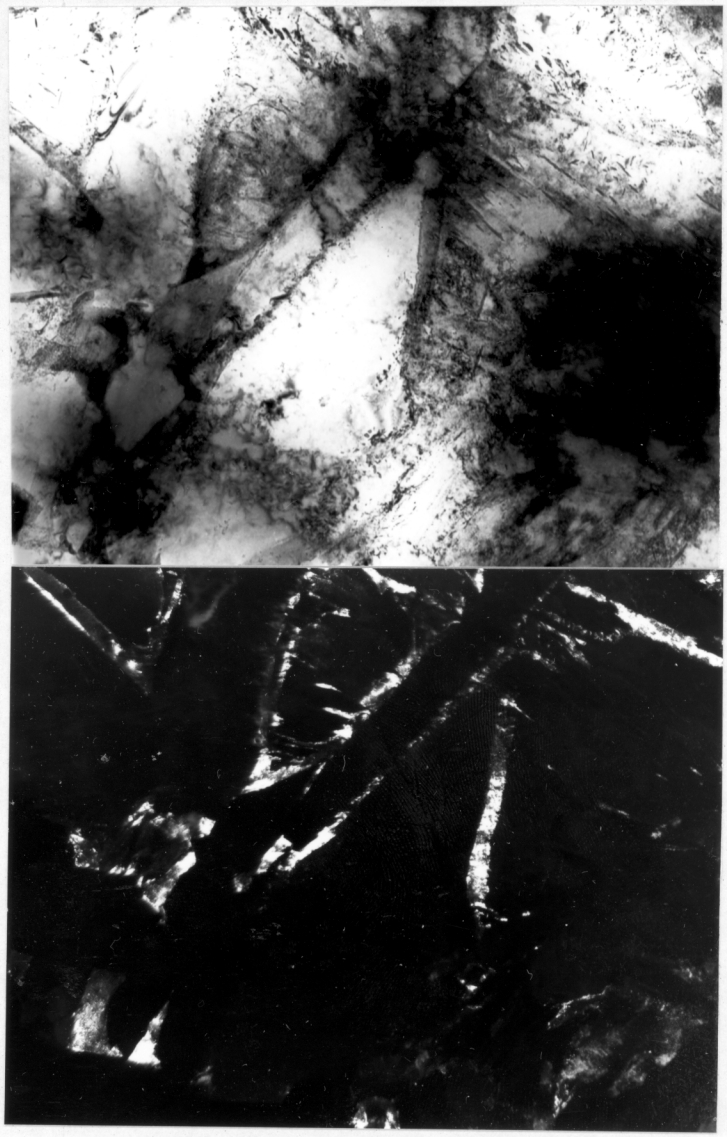

1.0μm

Figure 4.11. Bright and dark field images of retained austenite surrounding plates of acicular ferrite.

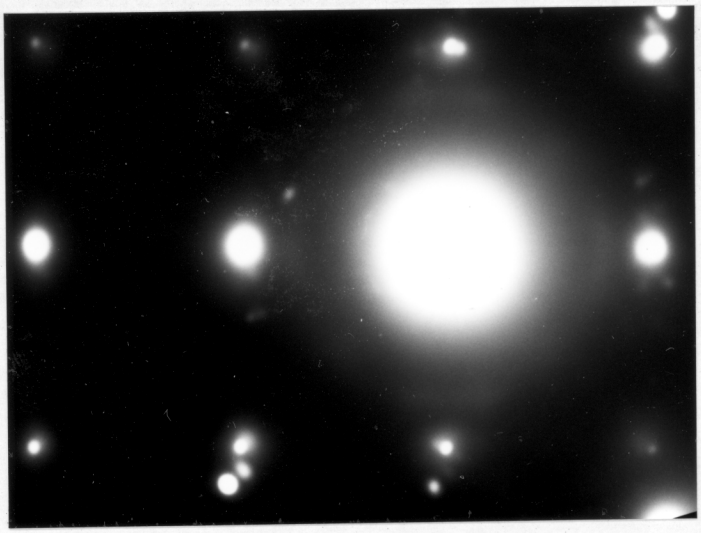

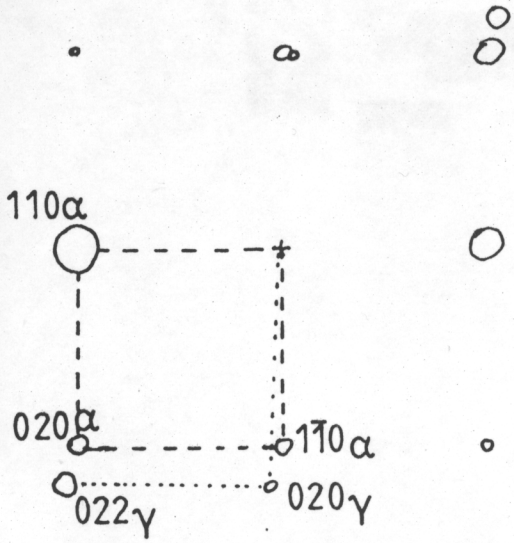

(a)

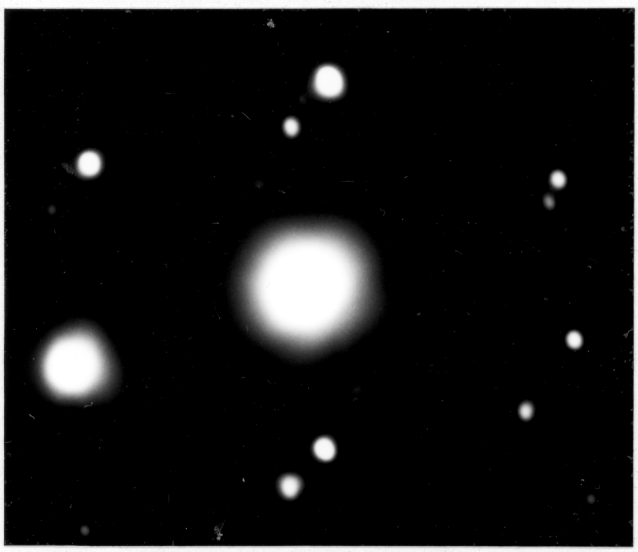

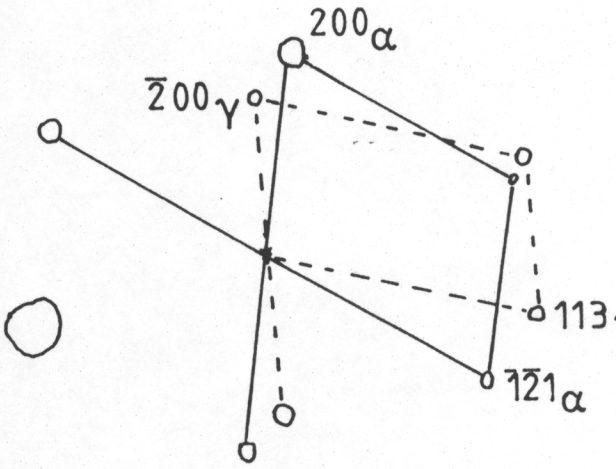

(b)

Figure 4.12. Selected area diffraction patterns from the α_{acic}/γ interface illustrating patterns from both phases. (a) is the SADP corresponding to figure 4.11.

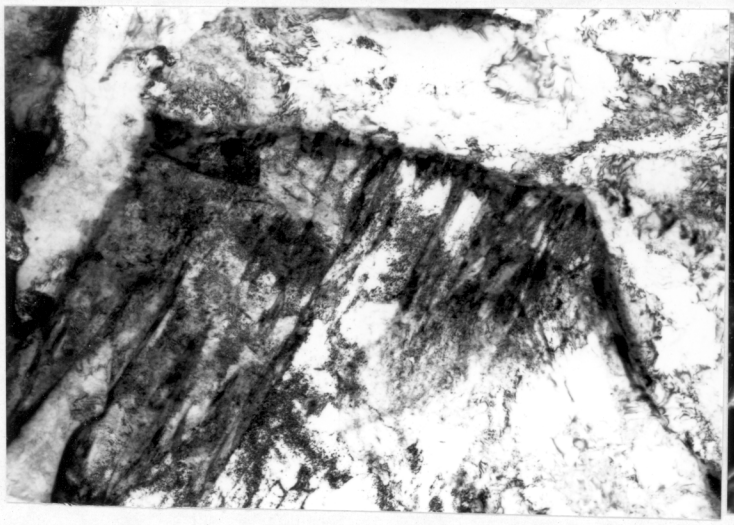

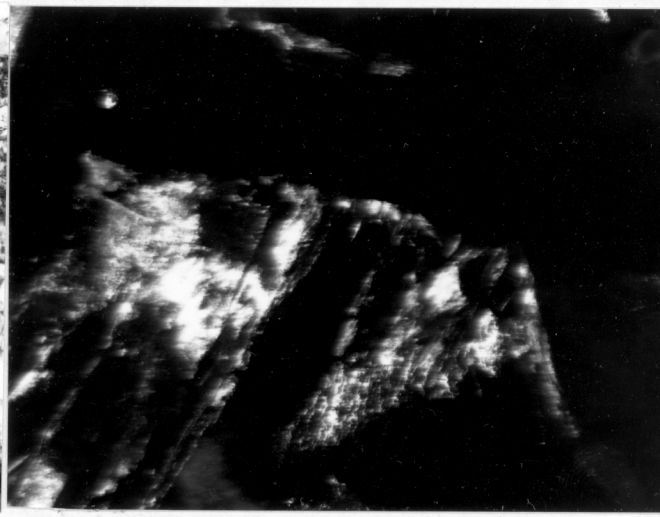

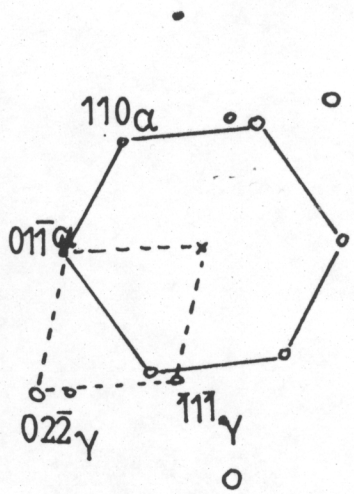

0.7μm

Figure 4.13. Further examples of retained austenite around α_{acic}.

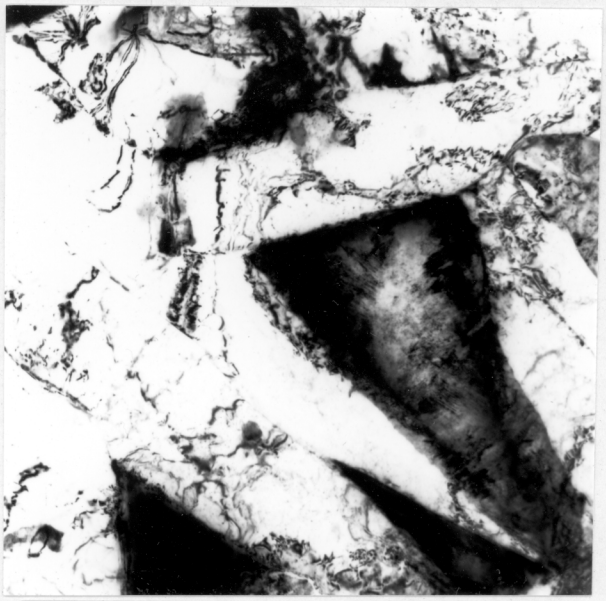

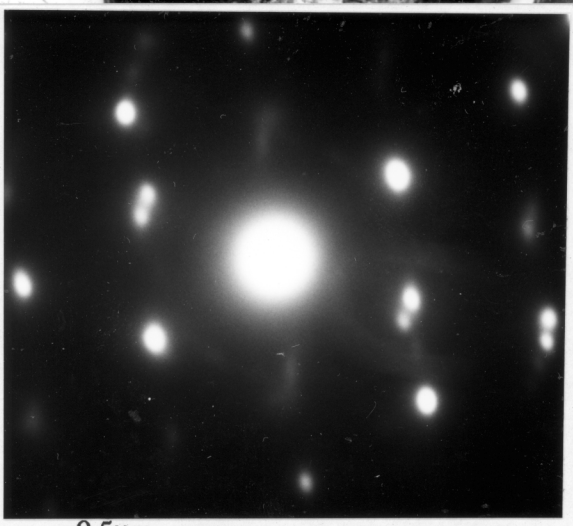

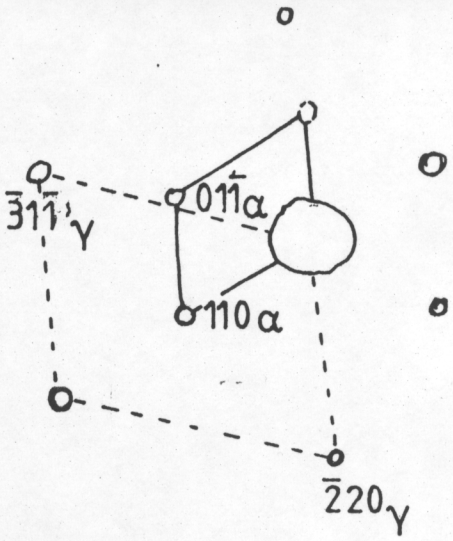

Figure 4.13 (continued).

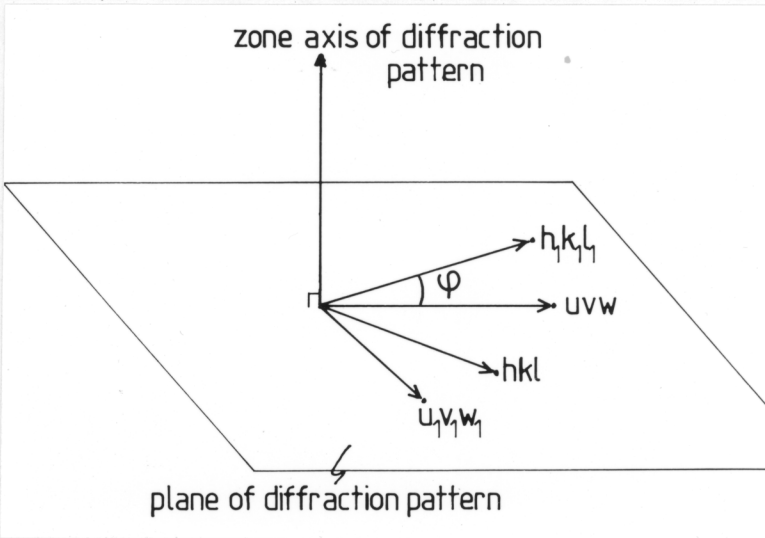

Figure 4.14. Analysis of α_{acic}/γ SADP's.

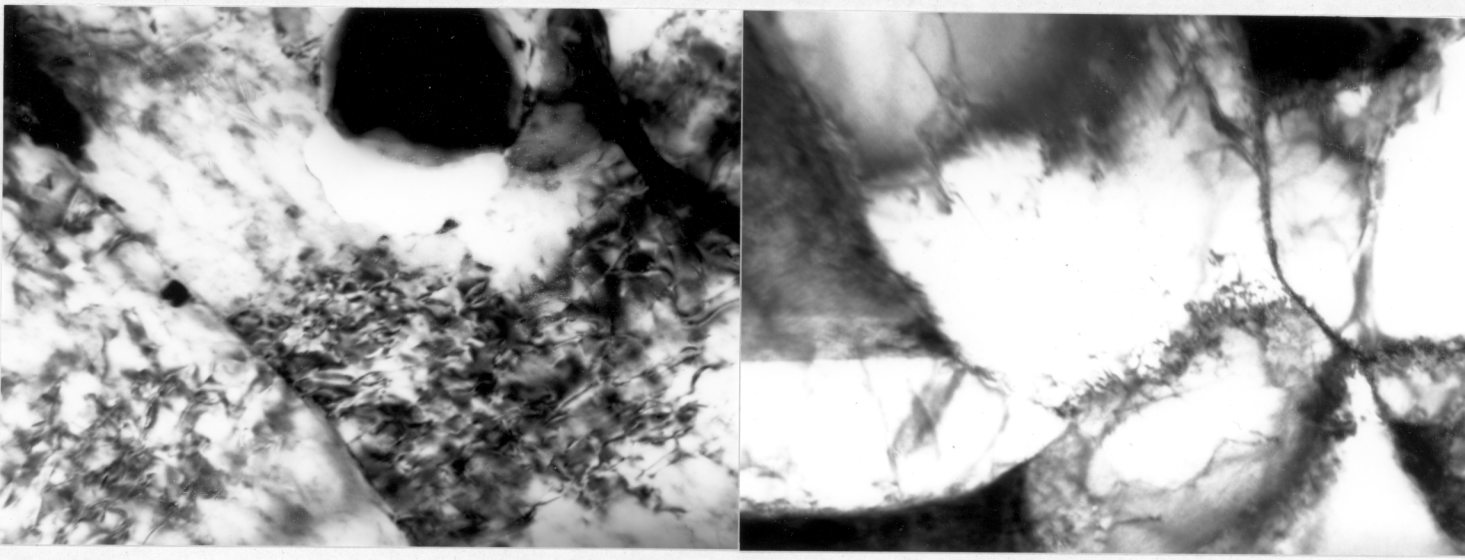

Figure 4.15. Increased dislocation density in central plate by hard impingement with adjacent plates.

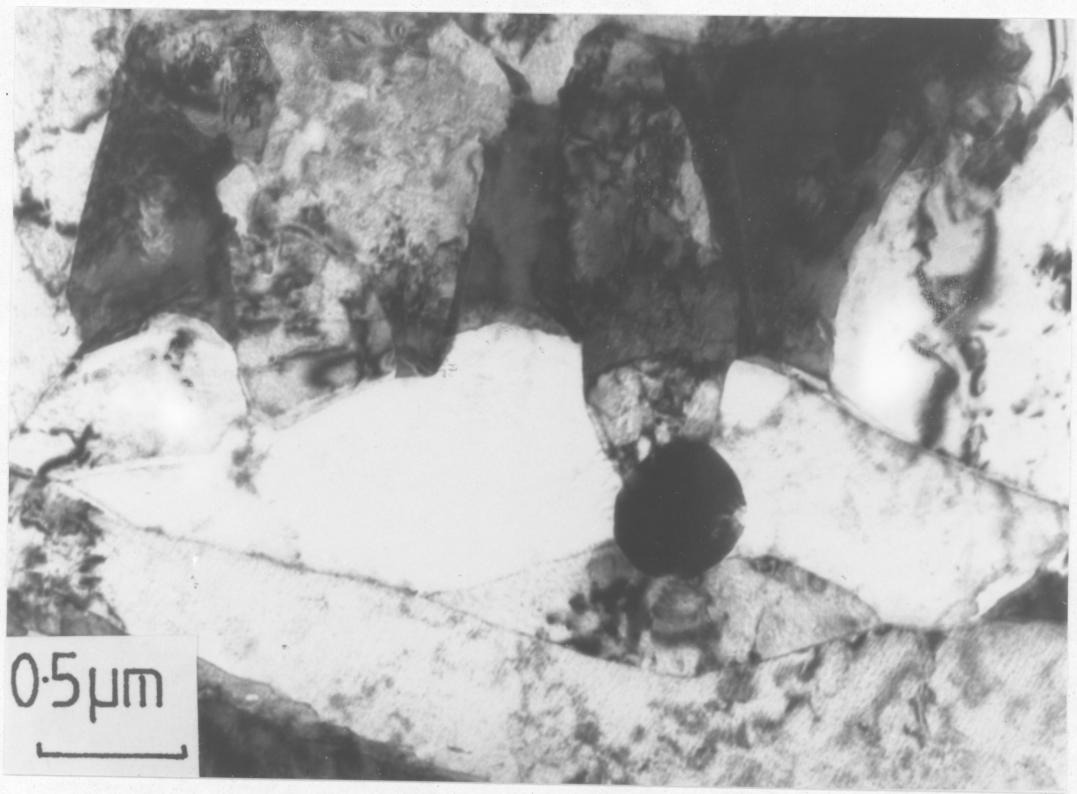

Figure 4.16. Multiple nucleation of plates on an oxide inclusion.

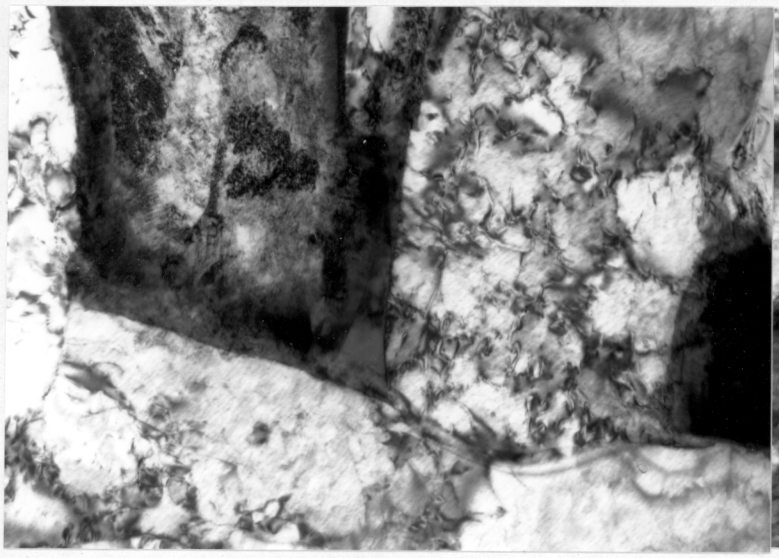

0.25μm

0.4μm

Figure 4.17. CSL lattice relations between α_{acic} plates separated by low angle boundaries.

10μm

Figure 4.18. Possible examples (arrowed) of sympathetic plate nucleation in PJ306 reaustenitised at 1200^{o}C for 10 minutes and isothermally treated at 439^{o}C for 40s.

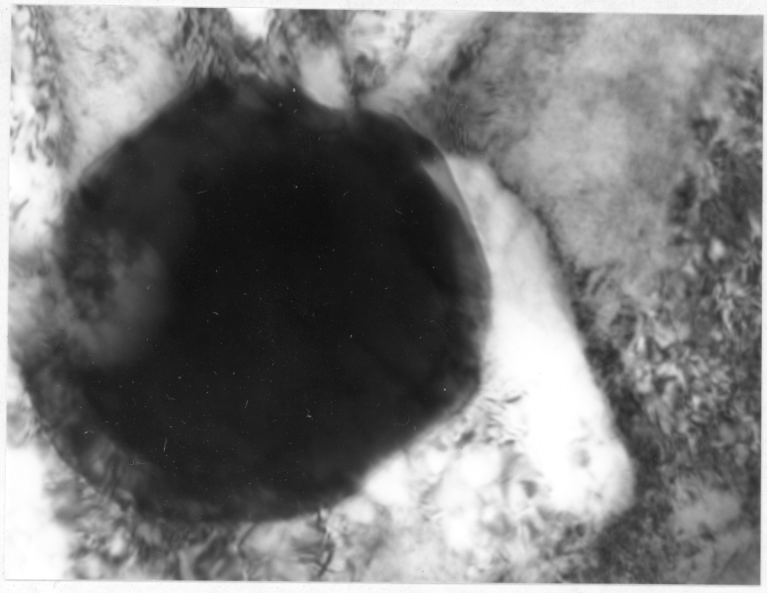

0.1μm

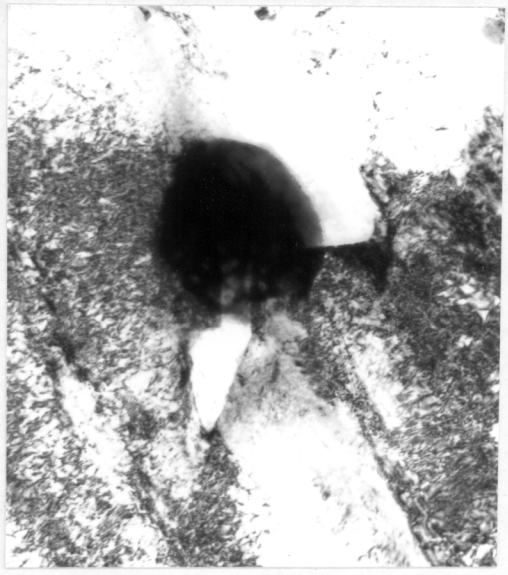

0.25μm

Figure 4.19. Initial formation of ferrite on weld inclusions.

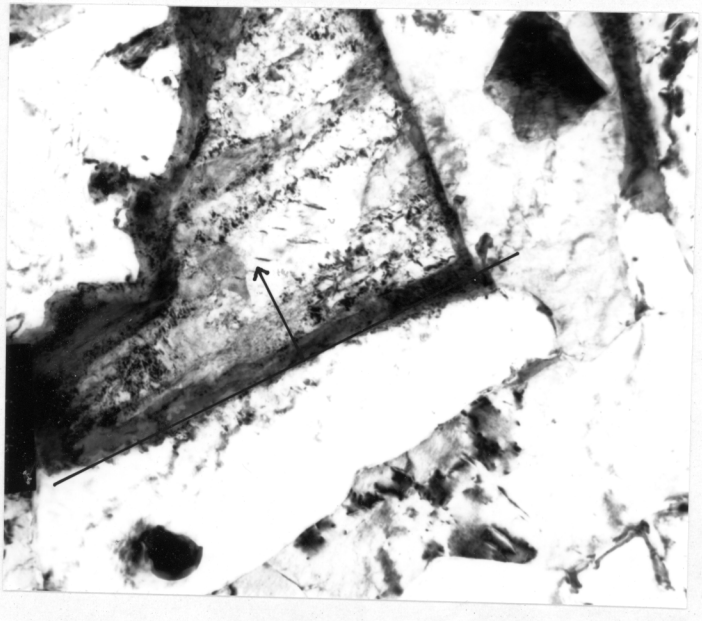

0.3μm

Figure 4.20. α_{acic} plates indicating mean interface traces and normals $\underline{n}(hkl)$.

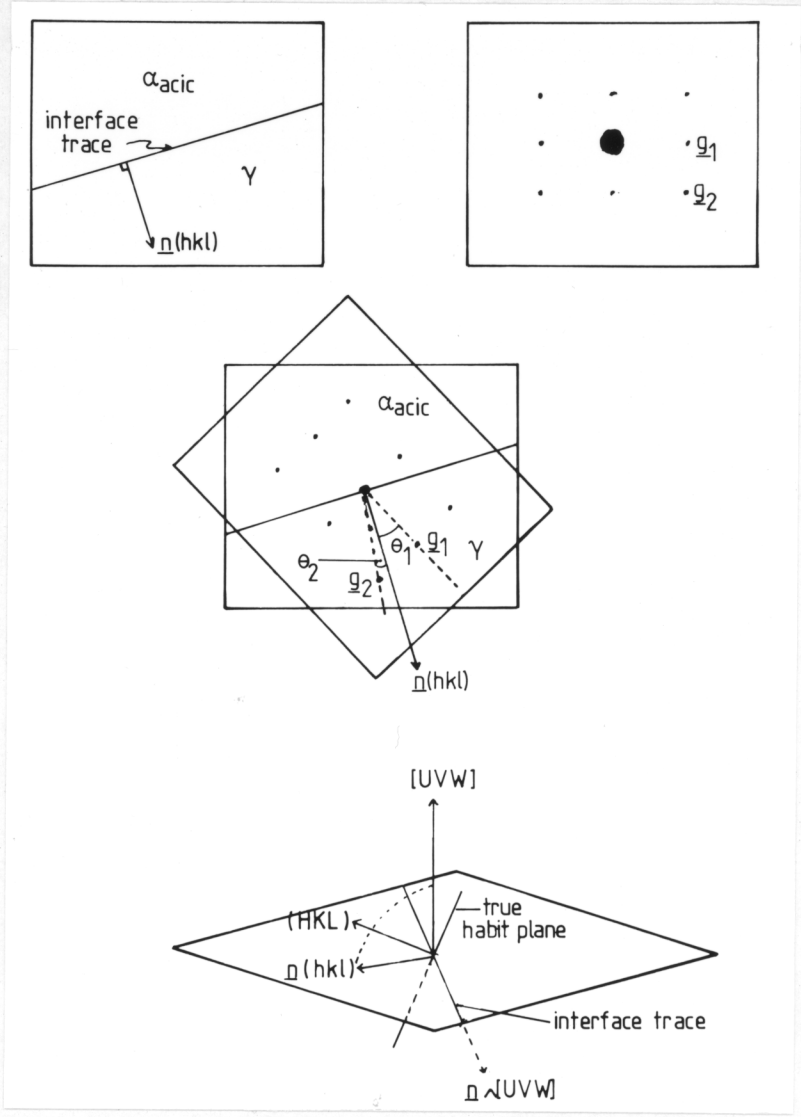

Figure 4.21. Stages in determination of γ/α_{acic} habit plane.

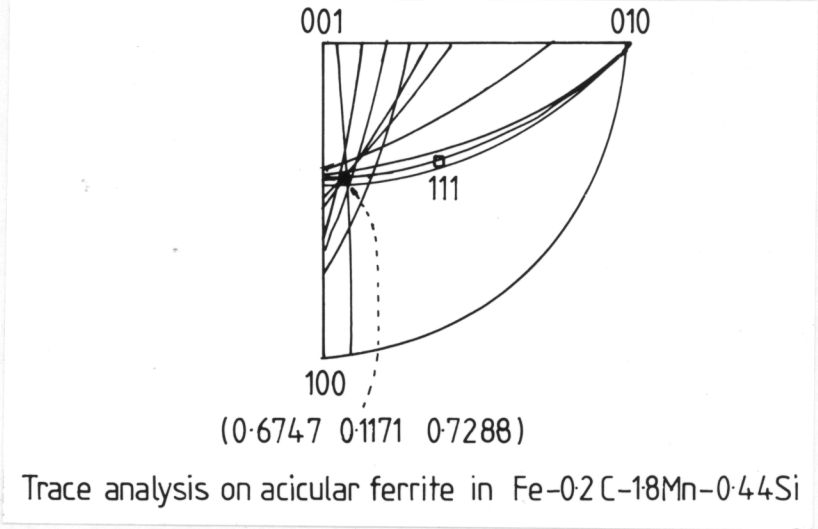

Figure 4.22. Stereogram showing great circles defined by $\underline{n}$(hkl) and [UVW].

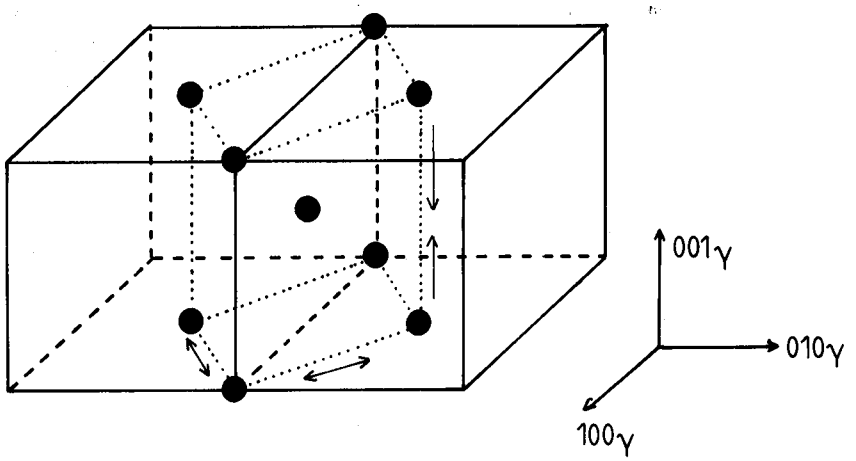

Figure 4.23. Formation of bcc unit cell from two fcc unit cells by action of Bain strain.

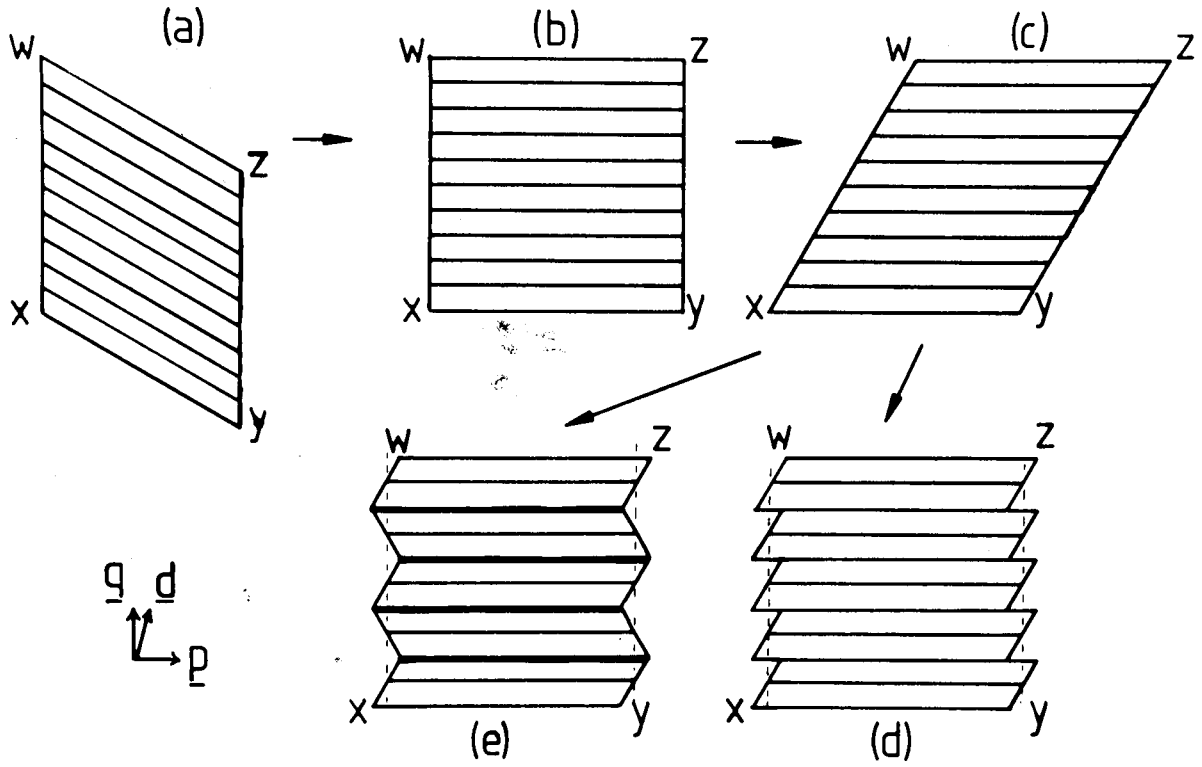

Figure 4.24. Stages in martensite formation.

4.25 (a). 486^{o}C, 60s. 10μm ——

(b) 490^{o}C, 50s. 10μm ——

4.25 (c). 490^{o}C, 60s. 10μm ——

(d) 493^{o}C, 100s. 10μm ——

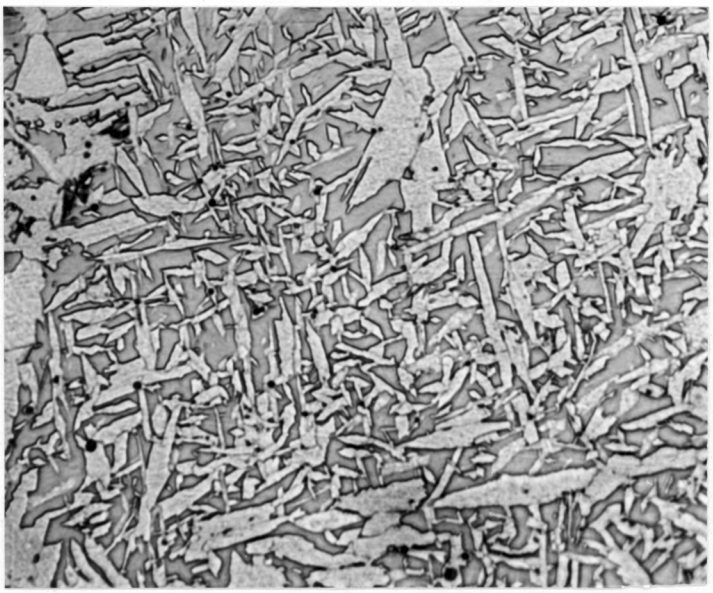

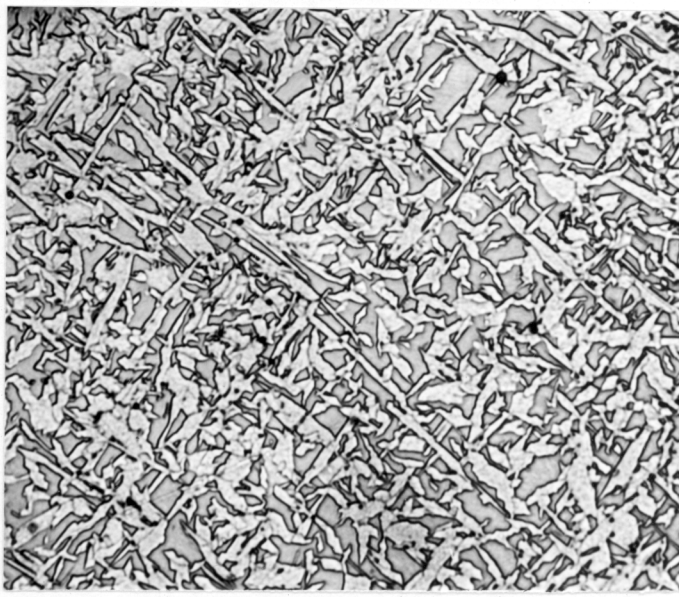

4.25 (e). 520^{o}C, 30s. 10μm ——

(f) 520^{o}C, 50s. 10μm ——

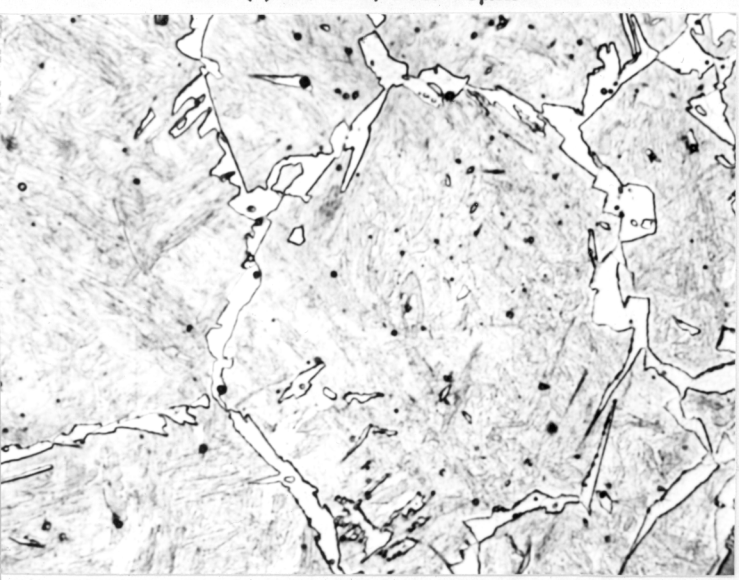

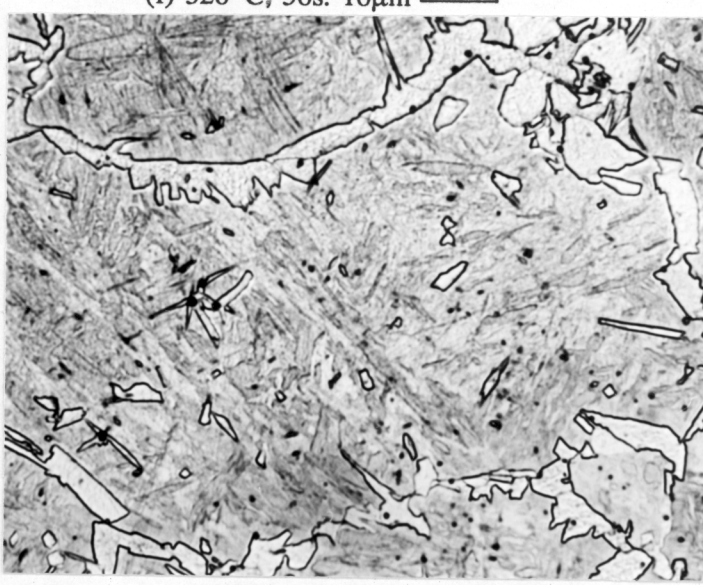

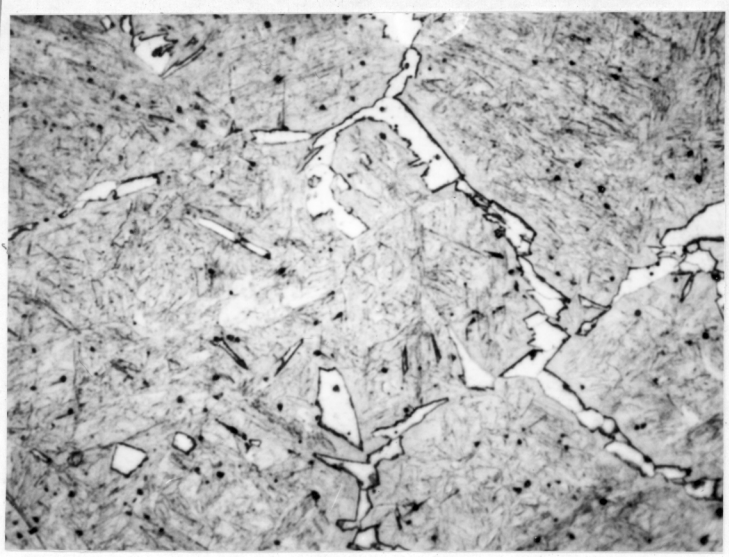

4.25 (g). 515°C, 60s. 10μm

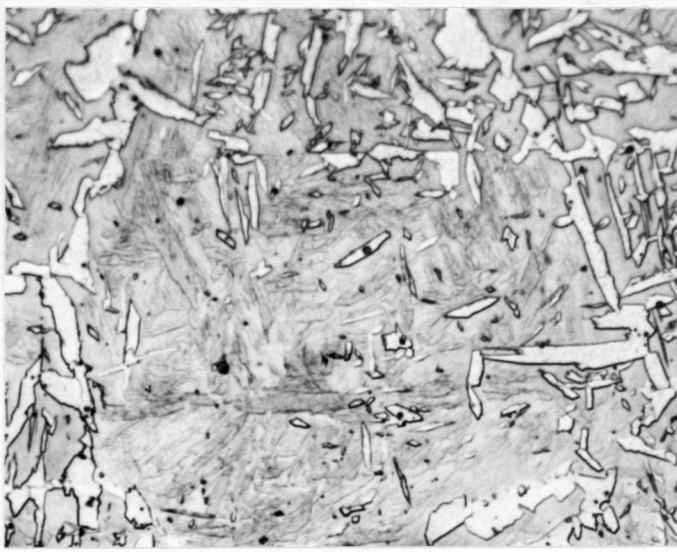

(h) 462°C, 30s. 10μm

4.25 (i). 460°C, 50s. 10μm

(j) 458°C, 60s. 10μm

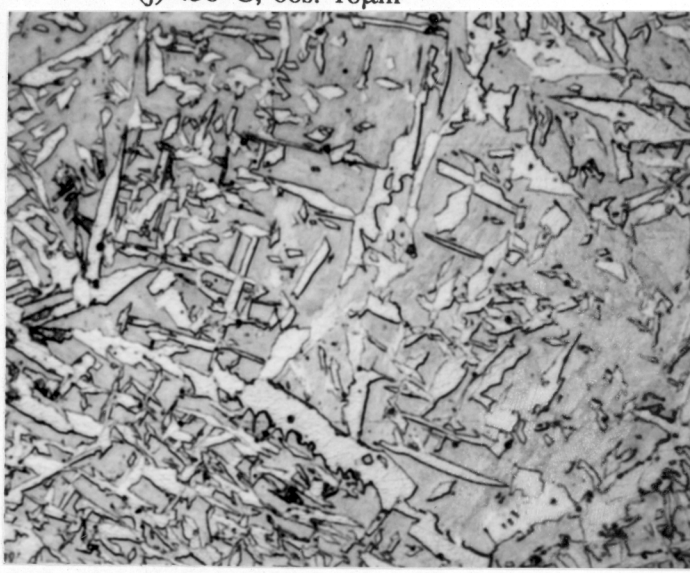

4.25 (k). 440°C, 30s. 10μm

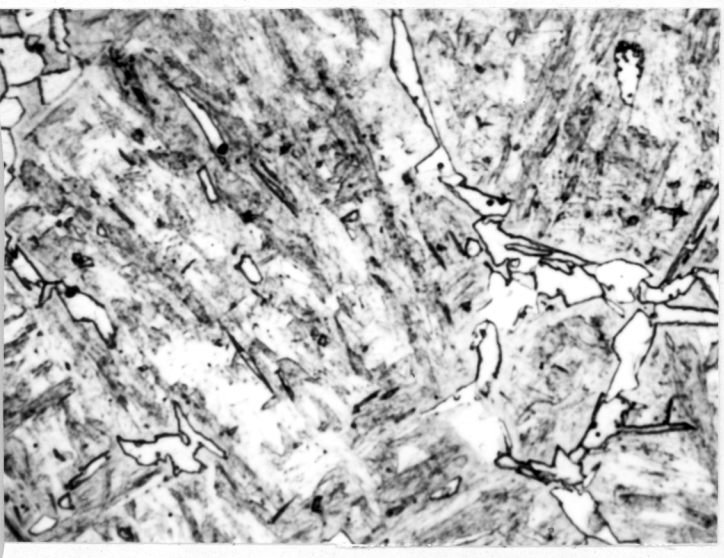

(l) 439°C, 40s. 10μm

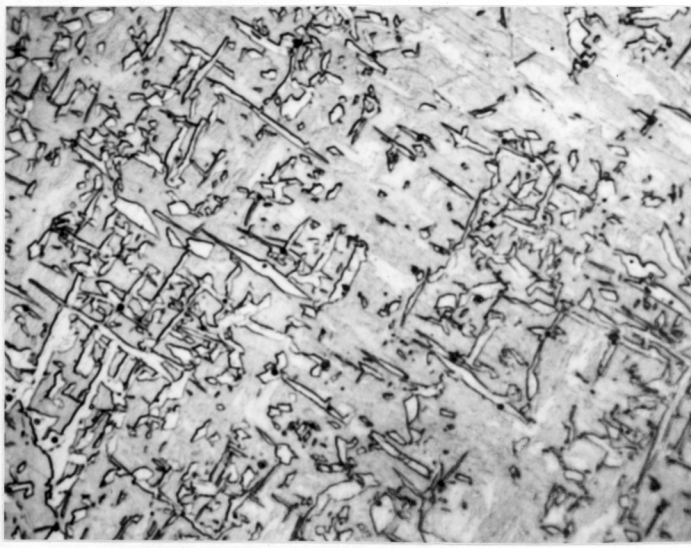

4.25 (m). 440°C, 50s. 10μm

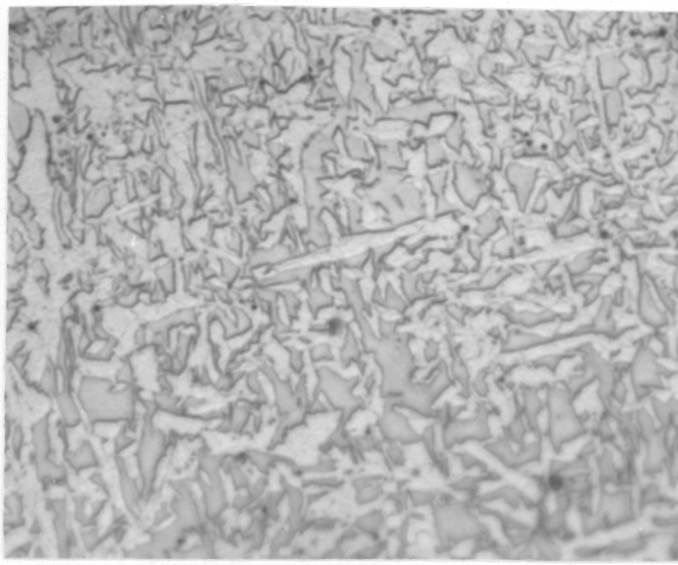

(n) 438°C, 60s. 10μm

4.25 (o). 435°C, 100s. 10μm

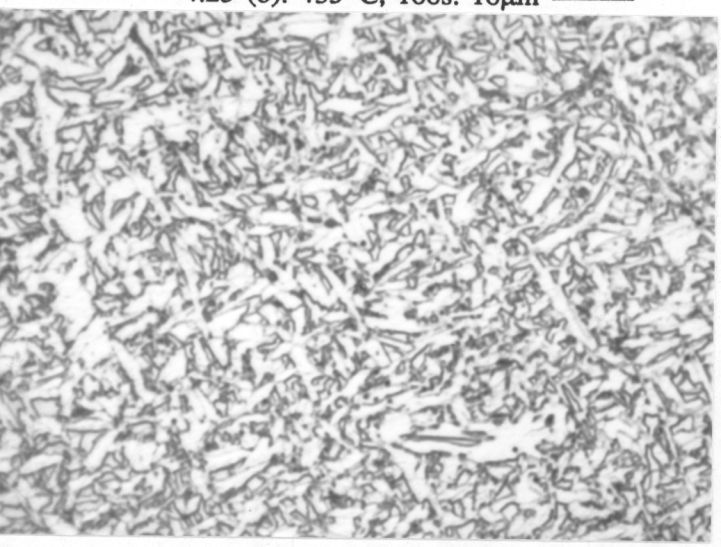

Figure 4.25. Microstructures resulting from various isothermal treatments of PJ306 after reaustenitisation at 1200°C for 10 minutes.

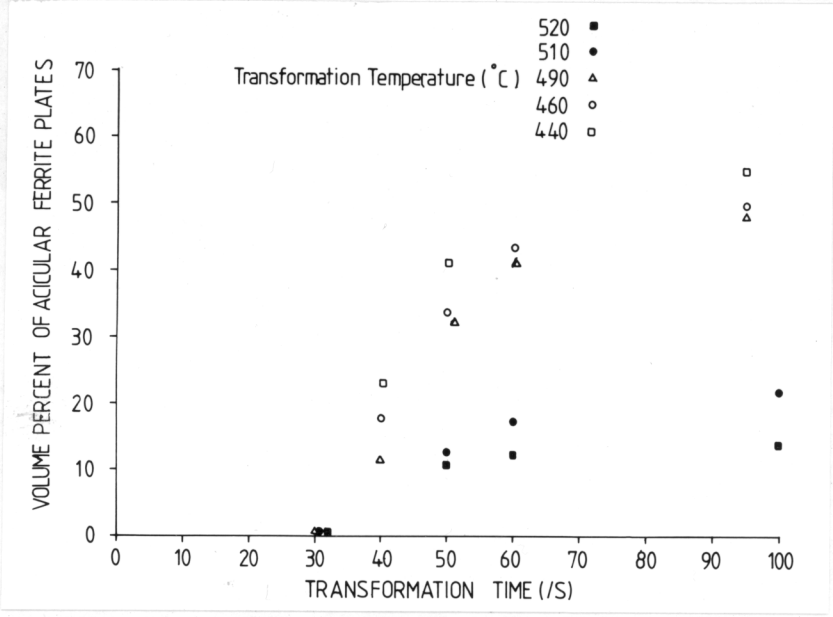

Figure 4.26. Transformation behaviour of α_{acic} as a function of time at various isothermal temperatures.

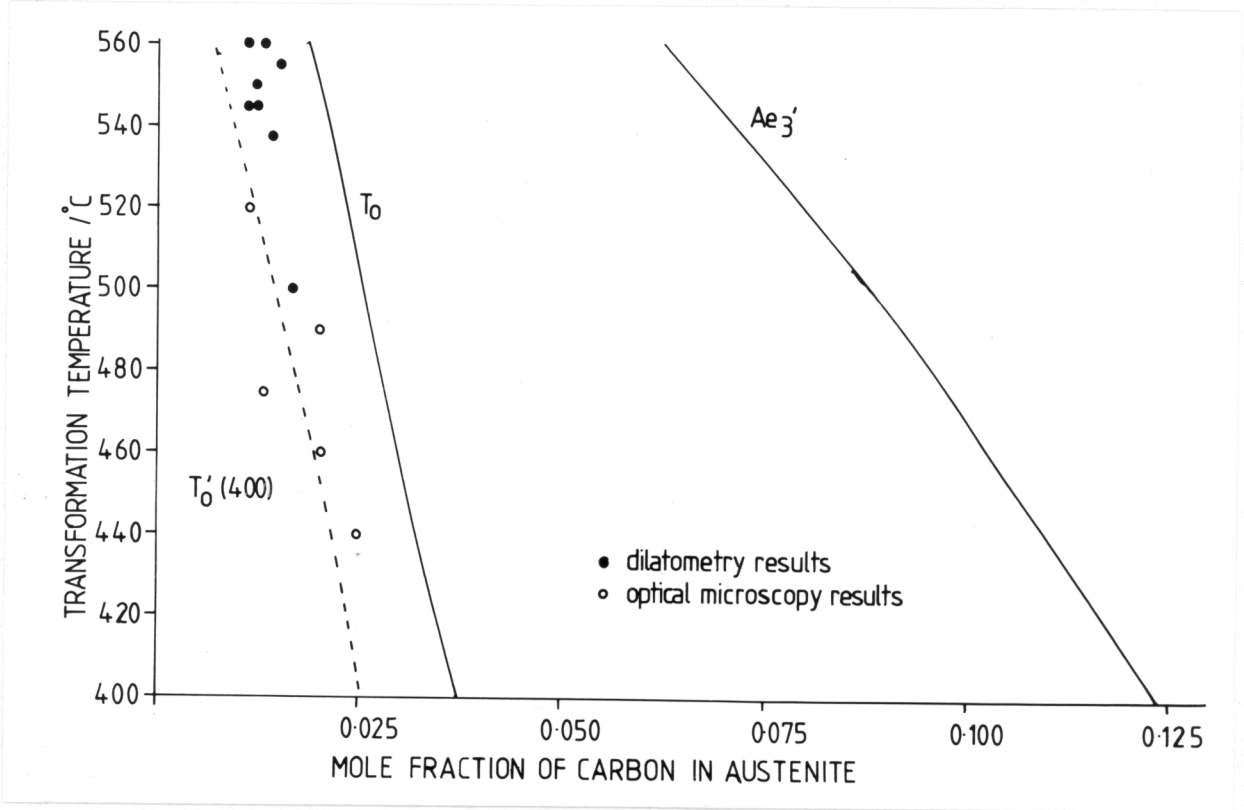

Figure 4.27. Mole fraction of carbon in γ as a function of transformation temperature at cessation of α_{acic} transformation.

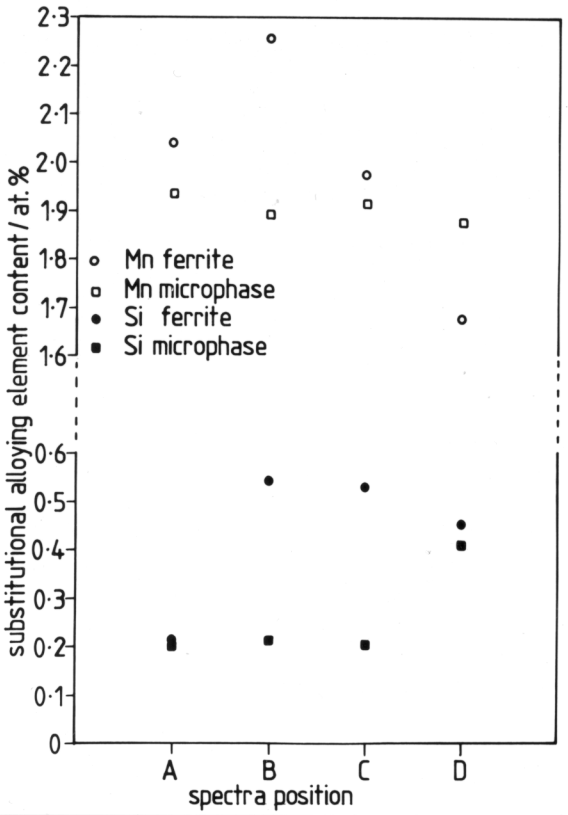

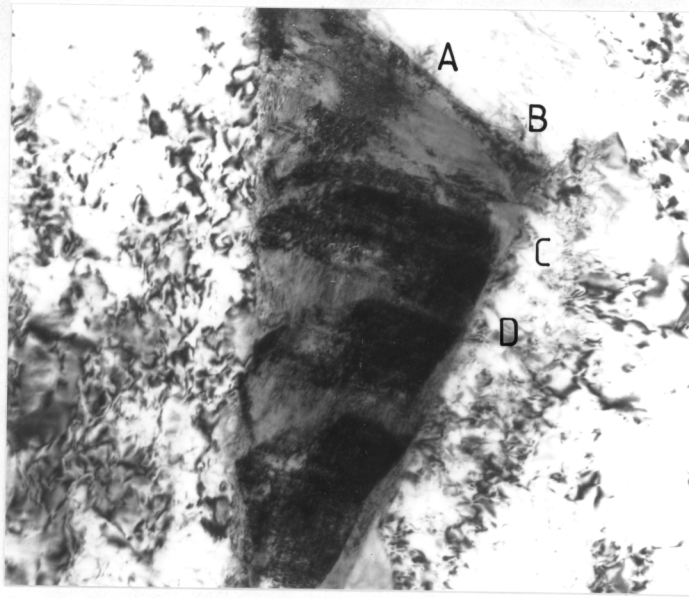

0.5μm

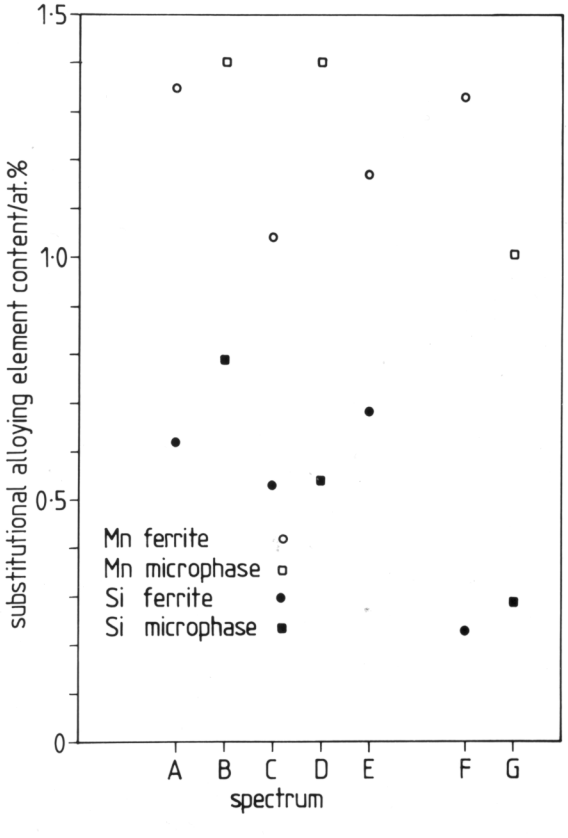

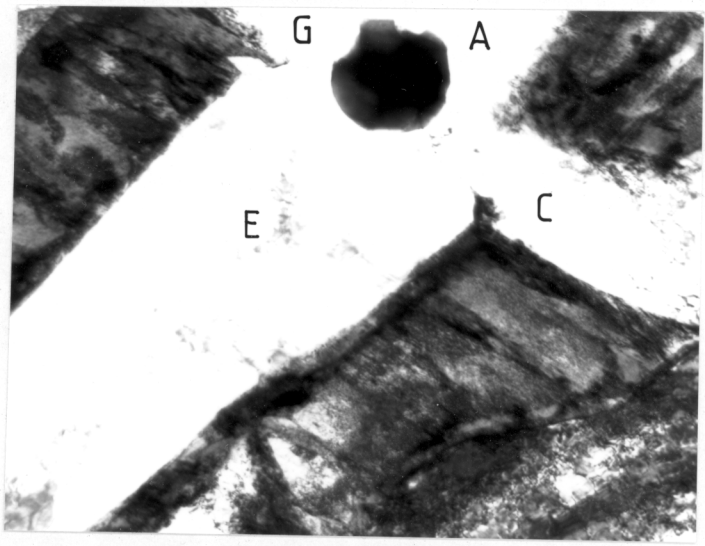

0.25μm

Figure 4.28. EDS plots and corresponding bright field images for α_{acic} and adjacent microphases.

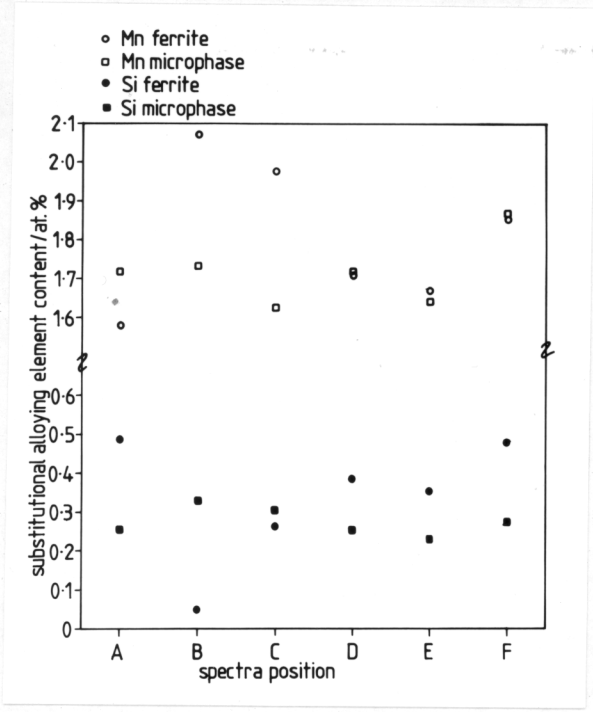

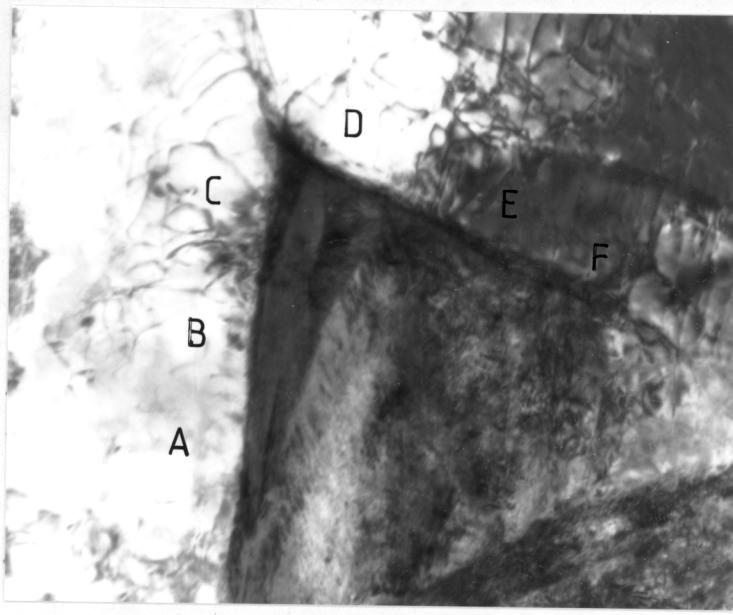

0.5μm

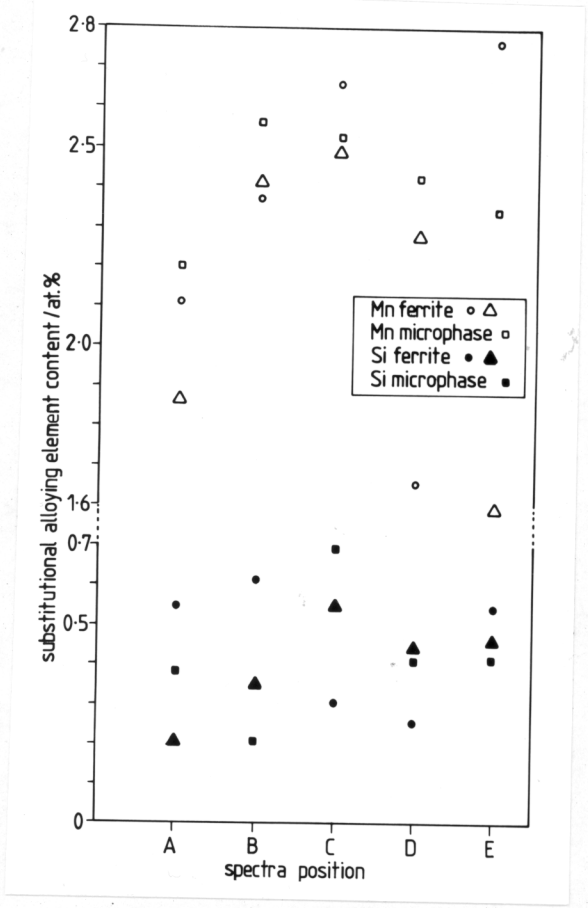

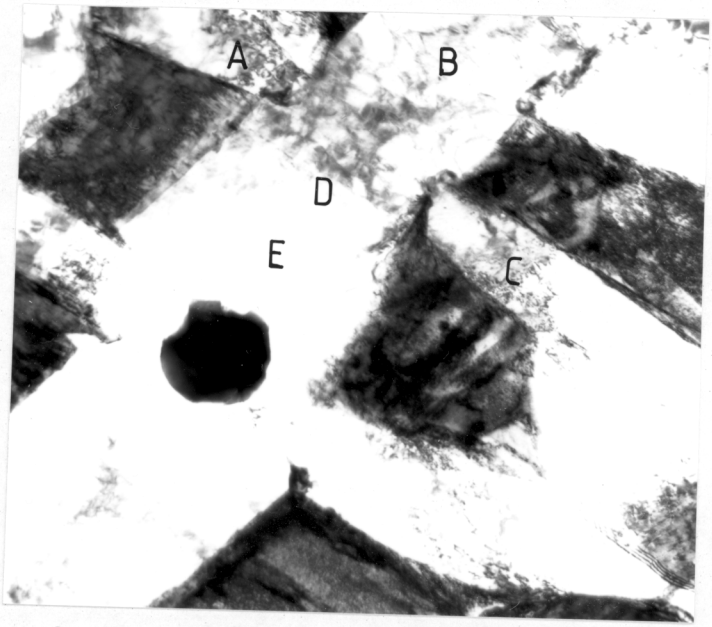

0.2μm

Figure 4.28 (continued).

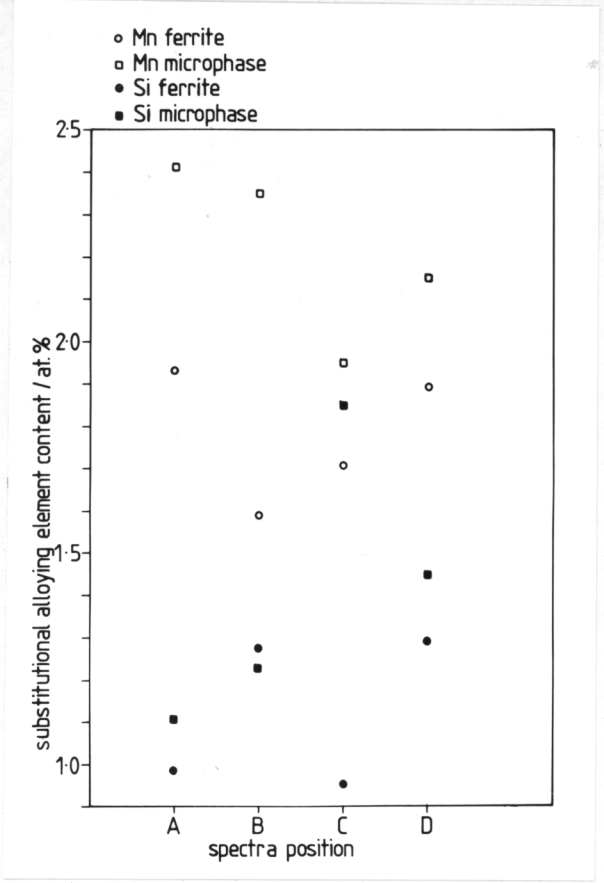

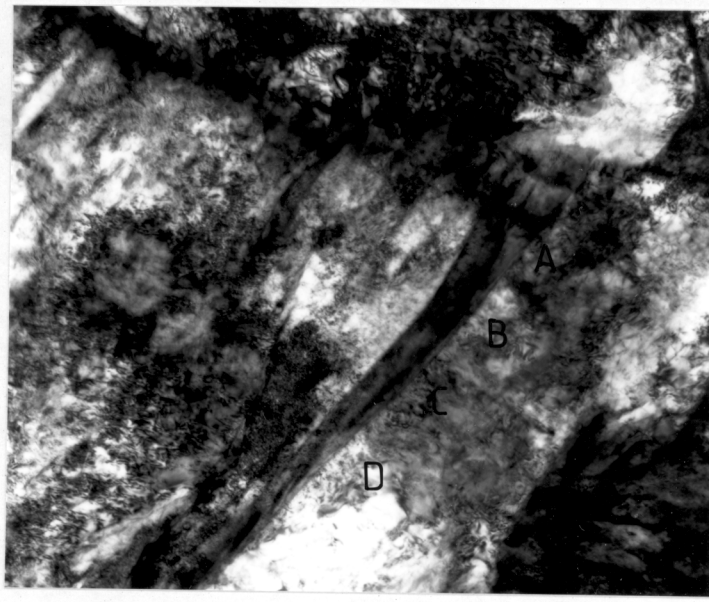

0.5μm

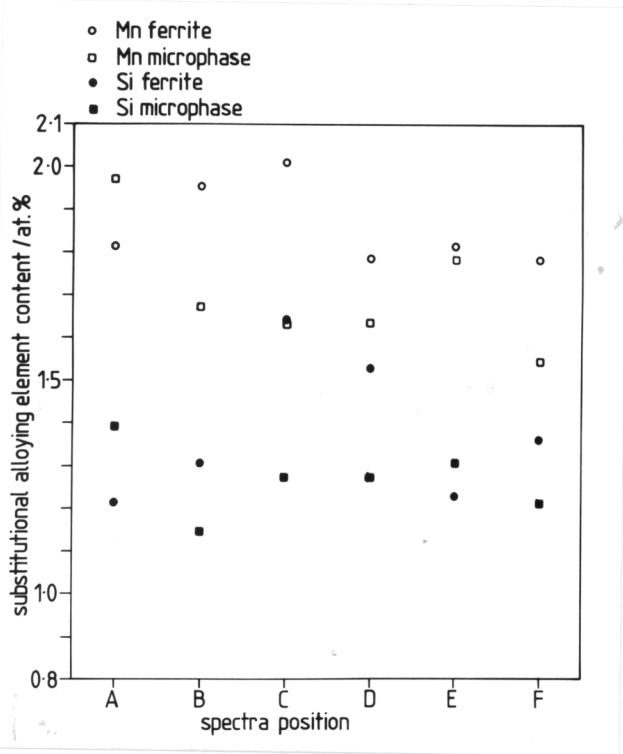

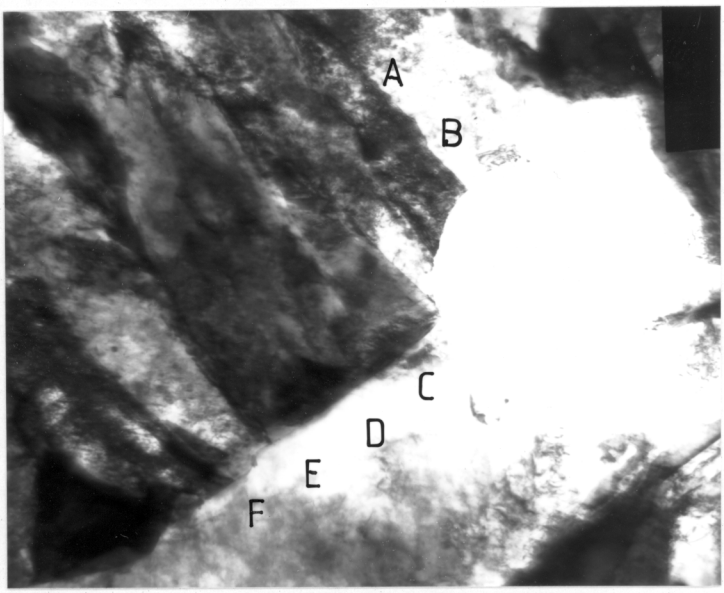

0.25μm

Figure 4.28(contd).